ACS APPLIED MATERIALS & INTERFACES
Research Article
www.acsami.org

Fabrication of $CuFe_2O_4/\alpha$-Fe_2O_3 Composite Thin Films on FTO Coated Glass and 3-D Nanospike Structures for Efficient Photoelectrochemical Water Splitting

Shabeeb Hussain,[†] Shazia Hussain,[†] Aashir Waleed,[‡] Mohammad Mahdi Tavakoli,[‡,§] Zilong Wang,[⊥] Shihe Yang,[⊥] Zhiyong Fan,[*,‡] and Muhammad Arif Nadeem[*,†]

[†]Catalysis and Nanomaterials Lab 27, Department of Chemistry, Quaid-i-Azam University, Islamabad 45320, Pakistan

[‡]Department of Electronic and Computer Engineering, Hong Kong University of Science and Technology, Clear Water Bay, Kowloon, Hong Kong SAR, China

[§]Department of Materials Science and Engineering, Sharif University of Technology, Azadi Street, Tehran 3716695349, Iran

[⊥]Department of Chemistry, The Hong Kong University of Science and Technology, Clear Water Bay, Kowloon, Hong Kong, China

Supporting Information

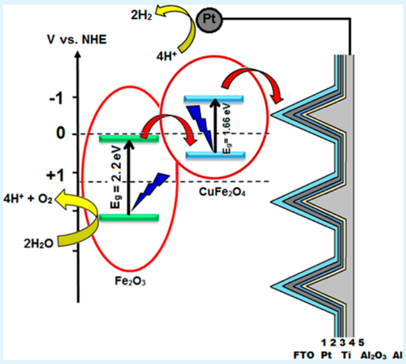

ABSTRACT: Recently, photoelectrochemical conversion (PEC) of water into fuel is attracting great attention of researchers due to its outstanding benefits. Herein, a systematic study on PEC of water using $CuFe_2O_4$/ $\alpha-Fe_2O_3$ composite thin films is presented. $CuFe_2O_4$/ $\alpha-Fe_2O_3$ composite thin films were deposited on two different substrates; (1) planner FTO glass and (2) 3-dimensional nanospike (NSP). The films on both substrates were characterized and tested as anode material for photoelectrochemical water splitting reaction. During PEC studies, it was observed that the ratio between two components of composite is crucial and highest PEC activity results were achieved by 1:1 component ratio (CF-1) of $CuFe_2O_4$ and $\alpha-Fe_2O_3$. The CF-1 ratio sample deposited on planar FTO substrate provided a photocurrent density of 1.22 mA/cm^2 at 1.23 V_{RHE} which is 1.9 times higher than bare $\alpha-Fe_2O_3$ sample. A significant PEC activity outperformance was observed when CF-1 ratio composite thin films were deposited on 3D NSP. The highest photocurrent density of 2.26 mA/cm^2 at 1.23 V_{RHE} was achieved for 3D NSP sample which is around 3.6 times higher than photocurrent density generated by $\alpha-Fe_2O_3$ thin film only. The higher photocurrent densities of 3D nanostructured devices compared to planar one are attributed to the enhanced light trapping and increased surface area for photoelectrochemical water oxidation on the surface. The difference between valence and conduction bands of $CuFe_2O_4$ and $\alpha-Fe_2O_3$ allows better separation of photogenerated electrons and holes at the $CuFe_2O_4$/ $\alpha-Fe_2O_3$ interface which makes it more active for photoelectrochemical water splitting.

KEYWORDS: *nanospikes, copper ferrite, hematite, ultrasonic spray pyrolysis, water splitting*

■ INTRODUCTION

The photoelectrochemical (PEC) water splitting is promising technology for the production of energy devices. In this context, hematite (α-Fe_2O_3) is considered a promising candidate to act as photoanode in PEC devices due to its suitable optical band gap (~2.2 eV),[1] which allows absorption of approximately 40% of solar flux. Moreover, its valence band position is suitable for O_2 evolution as a result of water oxidation reaction.[2] However, the conduction band of hematite has lower energy level than H^+/H_2 redox potential value, so reduction of water on the surface of hematite is not favorable. As a result, an external bias or coupling the hematite with solar cell is required to collect the photoexcited electron from the conduction band of hematite and transfer into the counter electrode to reduce the water. The valence band energy level of hematite is lower than O_2/OH^- redox potential. Thus, the holes produced in the valence band of hematite are capable to evolve O_2 by oxidation of water. It has been estimated that solar to hydrogen conversion efficiency of 16.8% can be achieved by using a semiconductor having similar optical band gap.[3] Practically, the lower solar to hydrogen efficiency of α-Fe_2O_3 is because of very short lifetime of photogenerated electrons and holes (<10 ps),[4,5] and their short diffusion length (~2−4 nm).[6] The above-mentioned problems associated with hematite are a big hurdle to make it applicable.

The alternative to hematite is ferrites, which is represented by general formula of MFe_2O_4, (M = Cu^{2+}, Zn^{2+}, Mg^{2+} etc.) and has many properties, which are desired for photoelectrolysis of water.[7] The ferrites are cheap, abundant, nontoxic, and have comparable band gap to α-Fe_2O_3. They can withstand in alkaline as well as in neutral environments. For instance, the use of $ZnFe_2O_4$ in photoelectrolysis as photo-

Received: September 30, 2016
Accepted: December 6, 2016
Published: December 16, 2016

DOI: 10.1021/acsami.6b12460
ACS Appl. Mater. Interfaces 2016, 8, 35315−35322

anode has been studied and reported several times; some reports demonstrated the pairing of $ZnFe_2O_4$ with semiconductors of wider band gap like TiO_2 can help to increase the visible light absorption.[8−10]

Among the spinel ferrites, the copper ferrite ($CuFe_2O_4$) is interesting due to its unusual property of phase transition, which also changes its semiconducting properties. In addition to its stability at higher temperatures, it also exhibits interesting electrical and magnetic properties.[11] Copper ferrite has been used in a variety of applications, such as gas sensing,[12] various catalytic applications,[13−15] and Li ion batteries.[16] Copper ferrite can absorb large part of the solar spectrum because of its narrow band gap with direct optical transition at 1.66 eV.[17] However, the large difference between the redox couple H_2O/H_2 and conduction band of $CuFe_2O_4$ (~1 V) leads to have poor photoactivity in hydrogen generation. The photogenerated charge separation in n-type α-Fe_2O_3 can be mediated by coupling with p-type $CuFe_2O_4$, which results in flowing of photoexcited electrons from conduction band of α-Fe_2O_3 toward valence band of $CuFe_2O_4$. The photoexcited electrons in α-Fe_2O_3 can follow Z−shaped path via valence and conduction band of $CuFe_2O_4$ to reach the outer circuit (Scheme 1). The combined effect of charge separation and mediation of electron flow toward the outer circuit can enhance the photocatalytic properties of α-Fe_2O_3. Only a few reports demonstrated the use of ferrites for thermochemical splitting of water to produce hydrogen and oxygen.[18−21] The use of $CuFe_2O_4$ as a photoanode is comparatively less studied than α-Fe_2O_3 due to difficulties faced in synthetic control for optimum atomic ratio.

Scheme 1. Schematic Representation of Energy Band Positions of $CuFe_2O_4/Fe_2O_3$ Dual-Absorber System

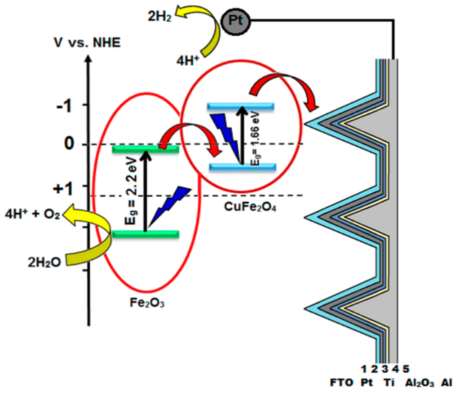

In this work, we report the deposition of $CuFe_2O_4/\alpha$-Fe_2O_3 composite thin films on FTO glass and NSP. The various thin films with different molar ratios of $CuFe_2O_4$ and α-Fe_2O_3 were fabricated and tested as anode materials for PEC water splitting. The highest PEC activity was achieved for 1:1 ratio of two components. The enhanced photocurrent density is attributed to the better separation of photogenerated electrons and holes at $CuFe_2O_4/\alpha$-Fe_2O_3 interface. The UV−vis results indicate that the ability of synthesized composite thin films to absorb the incident light is higher than pure α-Fe_2O_3. The light absorption increases with increasing the percentage of $CuFe_2O_4$ in $CuFe_2O_4/\alpha$-Fe_2O_3 composites (see Supporting Information). The performance of these composite thin films can be enhanced by depositing on 3D NSP due to higher surface area. In this case, a substantial increase in photocurrent density was observed and this behavior is attributed to the increased surface area and unique ability of 3D NSP to trap incident light extensively when compared to planar substrates.

As shown in Scheme 1, the "Z-shaped path" proposes direction of electrons toward the outer circuit. The conduction band of hematite and valence band of $CuFe_2O_4$ are well-aligned, which permit the flow of photoexcited electrons from conduction band of hematite to valence band of $CuFe_2O_4$. Thus, the holes generated in the conduction band of hematite only can oxidize water as its energy level is more positive as compared to oxidation potential of water. In fact, the aim of coupling of hematite with $CuFe_2O_4$ was to increase charge separation in hematite and to increase the conductivity by movement of photoexcited electrons from the conduction band of hematite toward the outer circuit via valence band and conduction band of $CuFe_2O_4$. So only holes in the valence band of hematite are responsible for photoelectrochemical water oxidation.

■ EXPERIMENTAL SECTION

Fabrication of 3D NSP Substrate. A 3D architecture of nanospike on aluminum foil was fabricated by using a previously reported method.[22] Briefly, aluminum foil was cut into pieces of 1.5 × 2.5 cm^2 area, sonicated for 10 min in isopropyl alcohol, rinsed by acetone, and dried by blower of compressed air. Aluminum chips were polished electrochemically where aluminum chips were used as an anode and carbon rod as a cathode. Both electrodes were dipped in the 1:3 (V: V) solution of perchloric acid and ethyl alcohol. A potential of 12 V was applied across the electrodes for 2 min at 10 °C. For patterned growth of anodized aluminum oxide (AAO), a 1 cm^2 Si mold of squarely ordered pillars with the height of 200 and 1200 nm pitch was used to get imprints over polished aluminum chips. The chips were imprinted by applying a pressure of 2×10^4 $N{\cdot}cm^{-2}$. Home made anodization setup was used to grow AAO under 480 V DC in a mixture of 9 mL of 0.1% (w/w) phosphoric acid, 240 mL of 1:1 (v/v) ethylene glycol and 2% (w/w) aqueous solution of citric acid. The anodization process was continued for 6 h at 10 °C using carbon rod as a counter electrode. To remove AAO, the anodized chips were dipped in the etching solution of 1.5% (w/w) of chromic acid and 6% (w/w) of phosphoric acid for 60 min at 98 °C. The resulting 3D NSP were rinsed with deionized water and dried with compressed air. To grow protective thin layer of Al_2O_3 against NaOH solution, the chips were anodized again at an applied potential of 20 V for 2 h in a solution of 3.4 wt% H_2SO_4. For extra protection of the device against basic electrolyte, a 100 and 50 nm thin layer of Ti and Pt was deposited over Al_2O_3 layer using magnetron sputtering. Finally flourine doped tin oxide (FTO) was deposited on the top of substrate using ethanolic solution of 0.2 M $SnCl_4$ and 0.04 M of NH_4F by ultrasonic spray pyrolysis (USP) technique. The mist of precursor solution produced in spinel atomization chamber of USP apparatus was decomposed at 450 °C with the aid of compressed air as a carrier gas which was controlled by mass flow meter.

Deposition of α-$Fe_2O_3/CuFe_2O_4$ Composite Layer on 3D NSP. Composite layers with different molar percentages of α-Fe_2O_3 and $CuFe_2O_4$ were deposited on the top of multilayer spiked structure by using ultrasonic spray pyrolysis (USP) technique. Ethanolic solution of appropriate molar ratios of $FeCl_3{\cdot}6H_2O$ and $CuCl_2{\cdot}2H_2O$ was used as precursor solution in which sodium citrate was added as a complexation agent. The

Table 1. Molar Concentration of the Precursor Solutions Used and Percentage Composition of $CuFe_2O_4/Fe_2O_3$ Composites Obtained from XRF Analysis

			composition: Fe_2O_3:CuO		composition: $CuFe_2O_4$:Fe2O3	
code	molar concentration of $FeCl_3·6H_2O$	molar concentration of $CuCl_2·2H_2O$	Fe_2O_3	CuO	$CuFe_2O_4$	Fe_2O_3
CF-5	0.02	0.05	85.2%	14.8%	1	5
CF-3	0.02	0.1	80.4%	19.6%	1	3
CF-2	0.02	0.15	74.7%	25.3%	1	2
CF-1	0.02	0.25	67.11%	32.89%	1	1

composition of the films was controlled by change in molar concentration of each precursor in the solution. It was observed that the vaporization rate of iron complex under sonication is much higher than Cu complex in the USP setup. So the deposition rate of Cu is quite low as compared to Fe. In order to adjust the ratio of $CuFe_2O_4$ in the composite, the concentration of Cu was kept much higher than Fe.

Deposition of $CuFe_2O_4/Fe_2O_3$ Composite Layer on FTO Coated Glass. FTO glass was cut in pieces of 1.5 × 2.5 cm^2 area and sonicated for 10 min in isopropyl alcohol, rinsed with acetone, and dried. Small portion of FTO glass was tightly covered by aluminum foil for wire connection and to avoid any deposition of metal oxide. By following similar procedure as deposition of $Fe_2O_3/CuFe_2O_4$ composite on nano spikes and by using similar precursors solutions mentioned in Table 1, $Fe_2O_3/CuFe_2O_4$ composite layers were also deposited on FTO glass. The optical images of prepared sample electrodes are shown in Figure S2 of Supporting Information.

Photoelectrochemical Studies. For photoelectrochemical studies, a single compartment standard cell consisting of three electrode system is used in which the sample devices were used as a working electrode, Ag/AgCl (4 M KCl) as a reference electrode and platinum coil as a counter electrode. The PEC measurements were carried out in 1 M aqueous solution of NaOH in dark and under irradiation (AM 1.5, 100 mW/cm^2). The beam of light was focused on front side of working electrode with 1 cm^2 exposed area. The measured potential values vs Ag/AgCl were expressed in reversible hydrogen electrode (RHE) scale by Nernst equation.

$$E_{\mathrm{RHE}} = E_{\mathrm{Ag+AgCl}} + 0.059\ \mathrm{pH} + E^{\circ}{}_{\mathrm{Ag/AgCl}}$$

Where E_{RHE} is the potential vs RHE, $E^{\circ}{}_{\mathrm{Ag/AgCl}}$ is the standard potential of Ag/AgCl reference electrode which is equal to 0.1976 V at 25 °C and $E_{\mathrm{Ag+AgCl}}$ represents the potential against Ag/AgCl reference electrode used.

■ RESULTS AND DISCUSSION

Characterization. The composition studies of thin films over FTO glass were made by using powder X-ray diffraction (XRD; Philips PW-1830) with Cu Kα radiation (λ = 1.5406 A). The X-ray diffraction patterns reveal that thin films deposited over FTO coated glass are of composite type and consist of α-Fe_2O_3 and $CuFe_2O_4$ components. The relative diffraction peak positions of $CuFe_2O_4$ are in accordance with standard diffraction pattern of $CuFe_2O_4$ (JCPDS 25-0283). There is no peak observed for copper oxides (CuO and Cu_2O). The peaks positioned at 2θ = 29.9°, 30.6°, 35.5°, and 43.1° were assigned as 202, 220, 311, and 400 reflections which belong to cubic spinel structure of $CuFe_2O_4$.[23] The diffraction peaks originated at 2θ= 26.5°, 33.6°, 37.8°, 51.5°, 54.4°, 61.5°, 66.6°, 78.5° are ascribed to 110, 101, 200, 211, 220, 310, 301, and 321, respectively, belonging to FTO.[24] While hematite (Fe_2O_3) is represented by diffraction peaks which are appeared at 35.5°, 40.9°, 49.4°, 62.4°, and 64° in PXRD pattern and are ascribed to 110, 113, 024, 214, and 300 reflections, respectively (Figure 1). Figure S5 shows the TEM image of $CuFe_2O_4$-α Fe_2O_3, indicating the interface between these phases. The interplanar spacing of $CuFe_2O_4$ and α Fe_2O_3 phases are 0.29 and 0.25 nm, which are corresponded to (220) and (110) planes, respectively. The results are consistent with XRD results.

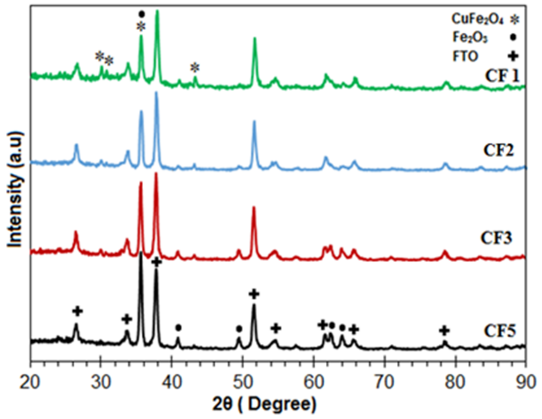

Figure 1. PXRD patterns of $CuFe_2O_4/Fe_2O_3$ composites deposited on FTO coated glass.

X-ray photoelectron spectroscopy (XPS) was used to investigate surface chemical composition of the $CuFe_2O_4$/Fe_2O_3 composite thin films. In Figure 2, full scan XPS spectra of composites CF-2 and CF-1 are given which reveal that Cu, Fe, and O are the main constituents in both the composites. XPS Cu 2p spectra of CF-1 and CF-2 could be fitted with one distinct doublet ($2p_{3/2}$ and $2p_{1/2}$) at about 934.2 and 954.0 eV which were the characteristics of Cu^{2+} species. The Cu^{2+} species could be further confirmed by the satellite peaks at 942 and 962 eV.[25] The binding energies centered at about 709.6 and 723.0 eV may be assigned to Fe^{2+}, and the binding energies in the region of 710.6−711.1 and 724.1−724.5 eV can be ascribed to Fe^{3+}. The binding energies centered about 713.3 and 726.7 eV are attributed to Fe^{3+} bonded with hydroxyl group (−OH).[26,27]

The O 1s peaks of both composites (CF-1 and CF-2) in Figure 2 are asymmetric and consist of intense peaks having a shoulder. It is considered that asymmetric peak is the combination of two peaks which may arise due to presence of two type of oxygen, one is chemically bound oxygen present in $CuFe_2O_4$/ α-Fe_2O_3 and other is the adsorbed oxygen. The asymmetric O 1s broad spectra of the CF-1 and CF-2 samples can be divided into four distinct peaks: peak (1) at 529.8 eV corresponded to metal−oxygen bonds; peak (2) at 531.2 eV attributed to −OH group; peak (3) at 532 eV assigned to C═O group; and peak (4) at 533.4 eV referred to multiplicity of

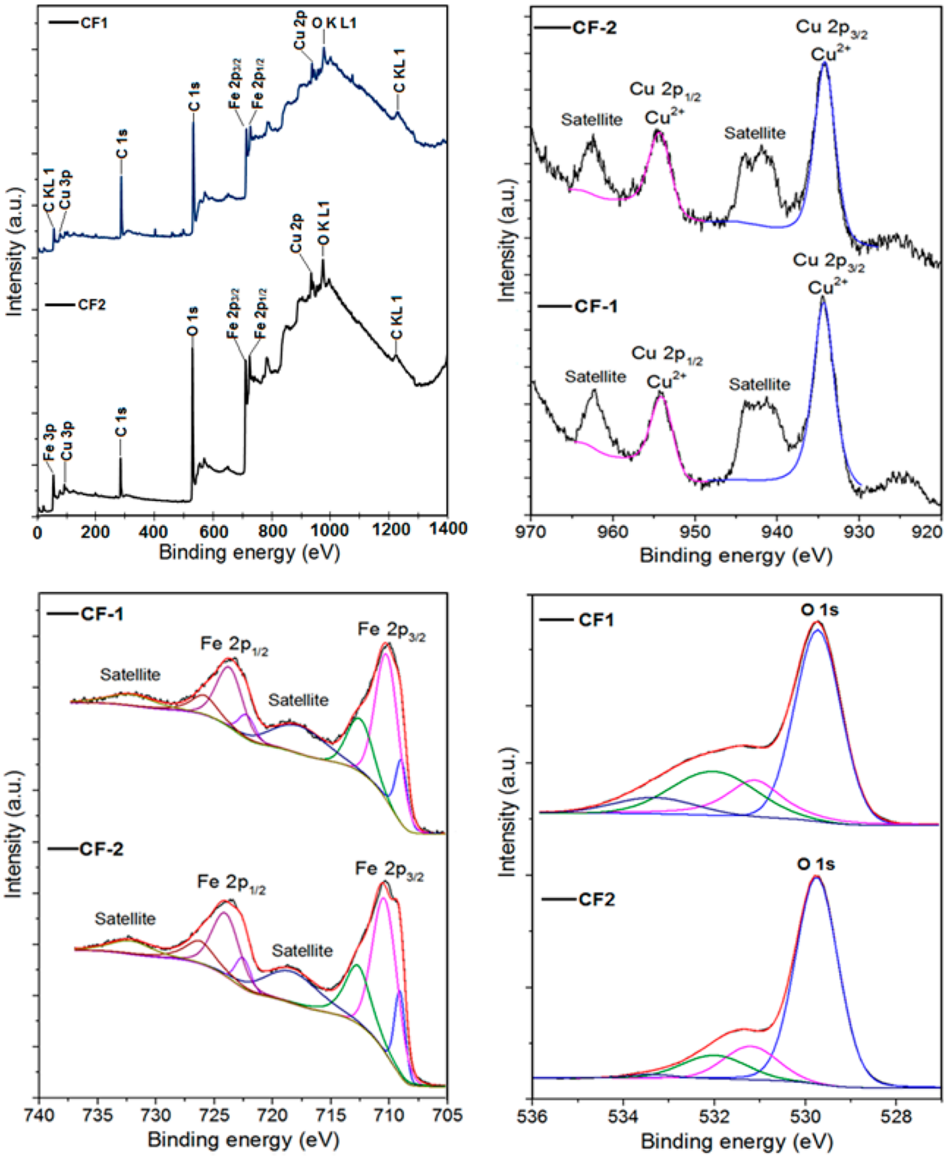

Figure 2. XPS spectra of composites CF-1 and CF-2.

physi- and chemi-sorbed water at the surface.[28] It has been explored that the amount of adsorbed oxygen in $CuFe_2O_4$ is larger as compared to α-Fe_2O_3. The exact ratio of Cu/Fe in the final composites was verified using X-ray fluororescence (XRF) technique and the results are demonstrated in Figure S1 of Supporting Information.

The ultrasonic spray pyrolysis set up which was used for fabrication of composite thin films, optical photograph of $CuFe_2O_4/Fe_2O_3$ thin film on FTO coated glass, and scanning electron microscopy images of $CuFe_2O_4/Fe_2O_3$ thin film at different magnifications are shown in Figure 3A–D. The morphology of $CuFe_2O_4/Fe_2O_3$ particles resembles with elongated and rice shaped structures. All the particles are homogeneously spread and their average grain size is ca. 100 nm. In magnified image, it can be visualized that grain density is high and the particles are also overlaying on one another. The results of elemental mapping using SEM technique further reveal the even distribution of Cu and Fe in the $CuFe_2O_4/Fe_2O_3$ thin film (Figure S3 of Supporting Information). Figure 4B is showing SEM image of nanospikes engraving on aluminum template after acidic anodization. A perfect ordering of nanospikes has been obtained by imprinting of polished aluminum chips using silicon mold consisting of ordered micro pillars in square fashion before anodization. The height of perfectly ordered nanospikes is ca. 1 μm. The overall pitch of this perfectly ordered nanospikes is 1.2 μm. Figure 4D is showing SEM view from the top of ordered nanospikes. The SEM image also shows that the evenly organized and ordered assembly of nanospikes can be viewed from all angles.

Figure 5A is showing top SEM view of well-organized nanospikes array after deposition of $CuFe_2O_4/Fe_2O_3$ composite by USP process. It is quite clear that USP process helps in smooth and uniform deposition of composite over NSP. To have a better estimation of uniform deposition of $CuFe_2O_4/Fe_2O_3$ composite, a zoomed top view of SEM image is provided in Figure 6B and C. The Figure 5D is demonstrating cross sectional SEM image of NSP coated with $CuFe_2O_4/Fe_2O_3$ composite which illustrates the layered structure (inset Figure 5D). The bottom layers (a) and (b) represent 100 nm Ti and 50 nm Pt film respectively, which were deposited by using sputtering technique for the purpose of electrode protection in basic electrolyte, i.e., 1 M aqueous NaOH solution. The layer

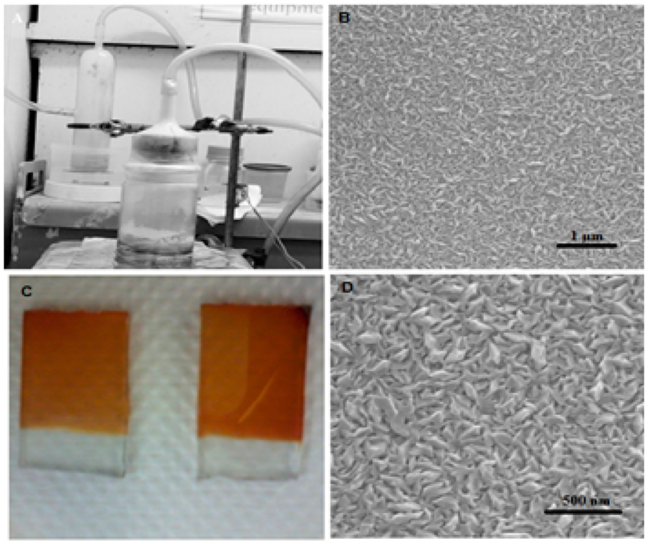

Figure 3. (A) Ultrasonic spray pyrolysis. (B) Photographs of $CuFe_2O_4/Fe_2O_3$ composite thin film on FTO coated glass while (C) low magnification and (D) high magnification SEM images of $CuFe_2O_4/Fe_2O_3$ composite thin film (CF-2).

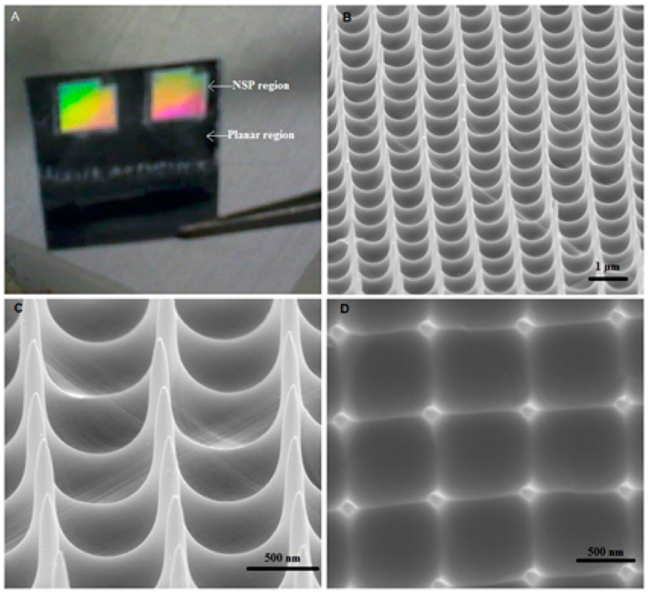

Figure 4. (A) An optical image showing planar region and nanospikes region on aluminum template. (B), (C) Low and high magnification SEM images of well-ordered nanospikes on aluminum chips. (D) SEM image showing top view of nanospikes on aluminum foil surface.

(c) is fluorine doped tin oxide (FTO) layer which is ca. 120 nm in thickness, while the top layer (d) is composed of $CuFe_2O_4/Fe_2O_3$ composite material.

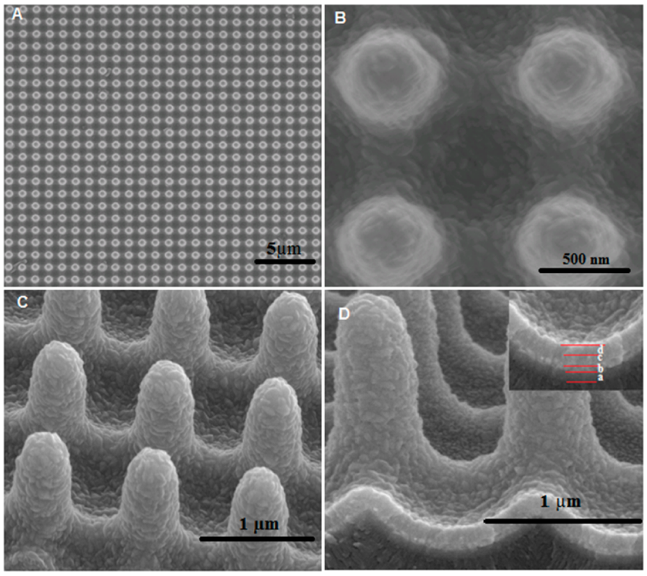

Figure 5. (A) Top view low magnified SEM image of perfectly ordered nanospikes array with composite $CuFe_2O_4/Fe_2O_3$ layer on the top. (B) High-magnification SEM image of the top view of nanospikes demonstrating evenly deposition of composite thin film. (C) 60-degree tilted view SEM image SEM image of NSP fully covered with $CuFe_2O_4/Fe_2O_3$ composite layer. (D) Cross sectional SEM image of final electrode. The inserted figure in cation shows the multilayer in detail. (A) Ti film having thickness of 100 nm, (B) 50 nm Pt thin film, (C) FTO thin film of about 120 nm thickness, (D) the top $CuFe_2O_4/Fe_2O_3$ composite layer having thickness around 80 nm.

Photoelectrochemical Studies. Figure 6 presents the linear sweep voltammograms (LSV) and photocurrent densities of fabricated thin films. The photocurrent densities of all devices were compared to pure hematite which was deposited on FTO coated glass. The Figure 6A shows the PEC *J*−*V* curves of $CuFe_2O_4/Fe_2O_3$ composite thin films deposited on FTO coated glass. The photocurrent densities of composite $CuFe_2O_4/Fe_2O_3$ sample electrodes were larger as compared to pure hematite. The $CuFe_2O_4/Fe_2O_3$ composite film deposited on FTO glass in which the ratio of $CuFe_2O_4$ and Fe_2O_3 was 1:1 (CF-1-Planar) exhibits highest PEC activity with the photocurrent density of 1.22 mA/cm^2 at 1.23 V_{RHE} which is 1.9 times higher than pure hematite (0.63 mA/cm^2). While the photocurrent densities of other composites thin films deposited on FTO coated glass CF-2-Planar, CF-3-Planar, and CF-5-Planar at 1.23 V_{RHE} were recorded as 0.99, 0.87, and 0.77 mA/cm^2, respectively. Figure 6B represents LSV of $CuFe_2O_4/Fe_2O_3$ composites deposited on 3D NSP. It was observed that the photocurrent densities generated by these films are significantly higher when compared with planar devices. The 3D nanostructures array offers large surface area for photoelectrochemical redox reaction and high optical absorption efficiencies which is ensuring increased light harvesting effect of the $CuFe_2O_4/Fe_2O_3$ composite films. The distance between the two neighboring $CuFe_2O_4/Fe_2O_3$ coated nanospikes is ca. 400−500 nm which is comparable to the wavelength of the incident visible light which causes the increased absorption of light as a result of diffraction effect.[29] Notably, the photocurrent density of the 3D nanostructured device covered by highly active $CuFe_2O_4/Fe_2O_3$ composite (CF-1-NSP) at 1.23 V_{RHE} was 2.26 mA/cm^2 which is some 1.85 times higher value than that obtained from planar device with similar photoactive composite thin film. The highly active composite film deposited on NSP (CF-1-NSP) exhibits 3.6 times higher photocurrent density as compared to pure hematite thin film on FTO coated glass. It can be seen that the dark current for 3D nano structured electrode at 1.23 V_{RHE} is nearly zero which means that conductive protective layer of platinum was completely covered by FTO film followed by $CuFe_2O_4/Fe_2O_3$ composite thin film and it is the photoactive composite layer which is generating photocurrent solely upon illumination. In dark condition when the applied voltage goes beyond 1.7 V vs RHE,

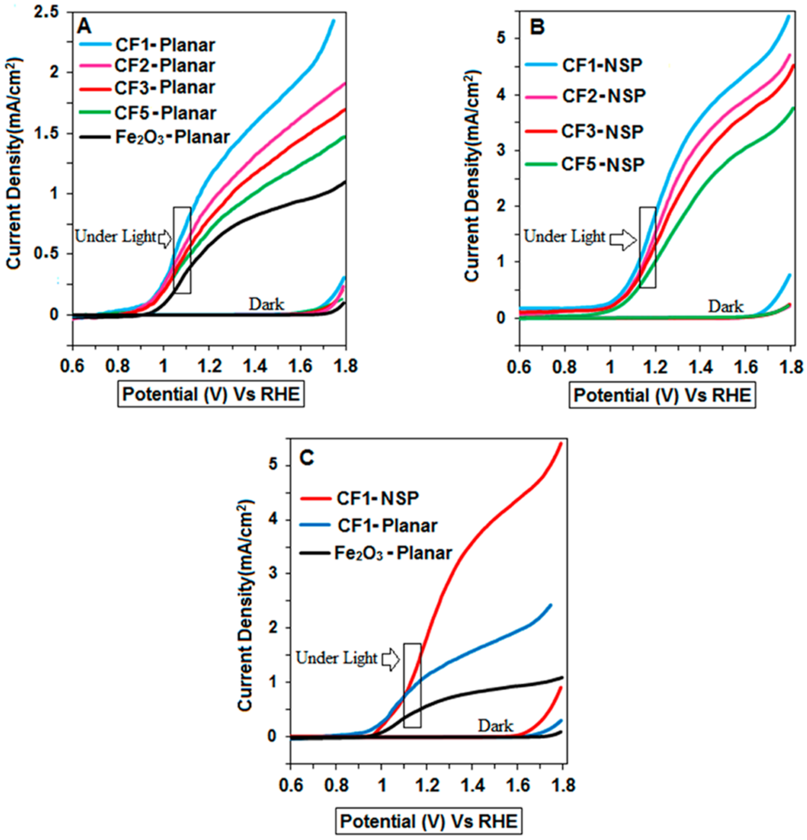

Figure 6. (A) Linear sweep voltammograms (LSV) of $CuFe_2O_4/Fe_2O_3$ composites deposited on planar FTO coated glass. (B) LSV curves of $CuFe_2O_4/Fe_2O_3$ composites deposited on 3-D nanospikes. (C) A comparison of photocurrent density of CF-1-NSP with CF-1-Planner and hematite-Planner.

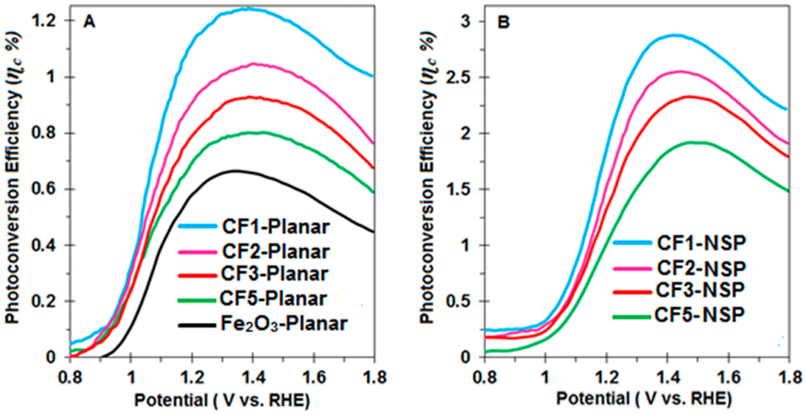

Figure 7. Plot of energy conversion efficiency (ECE) η_c versus applied potential. The applied potential was calculated according to the equation, $E_{app} = E_{meas} - E_{ocp}$.

the oxidation reaction on working electrode get started and increased with increase of applied voltage. Upon illumination of working electrode by solar simulator the water oxidation reaction started even below 1.23 V vs RHE due to photogenerated holes in the composite while electrons flow toward the outer circuit which result the net gain in photocurrent density.

The photoconversion efficiency (η_c) was calculated by using eq 1 and the results are shown in Figure 7.

$$\eta_c(\%) = \frac{Jp[(E^{\circ}rev - |E_{app}|)]}{I\ (light)} \times 100 \qquad (1)$$

Where η_c represents photoconversion efficiency, Jp denotes the photocurrent density, E°_{rev} is the standard reversible potential (1.23 V vs RHE), E_{app} is the applied potential ($E_{app} = E_{meas} - E_{ocp}$, where E_{meas} is the potential of working electrode vs Ag/AgCl and E_{ocp} represents the potential (vs Ag/AgCl) of working electrode under open circuit condition), and I (light) is the intensity of incident light which is equal to 100 mW/cm^2.

Among the planar devices the CF-1-Planar showed the maximum value of photoconversion efficiency η_c (1.24%) at 1.35 V vs RHE (0.355 V vs Ag/AgCl) which is 1.85 time higher value compared to pure hematite (η_c = 0.67%). The photoconversion efficiency (η_c) of 3D nanostructured device

Table 2. Comparison of Photocurrent Density and Photoconversion Efficiencies of Pure Hematite with the $CuFe_2O_4/Fe_2O_3$ Composites Deposited at Two Different Substrates

device codes	type of device	composition: $CuFe_2O_4$:Fe_2O_3	photocurrent density (mA/cm^2) at 1.23 V vs RHE	photoconversion efficiency (η_c)
Fe_2O_3	planar	pure hematite	0.63	0.67%
CF-1-Planar	planar	1:1	1.22	1.24%
CF-2-Planar	planar	1:2	0.99	1.04%
CF3-Planar	planar	1:3	0.87	0.92%
CF-5-Planar	planar	1:5	0.77	0.80%
CF-1-NSP	3D nanostructured	1:1	2.26	2.87%
CF-2-NSP	3D nanostructured	1:2	1.81	2.54%
CF-3-NSP	3D nanostructured	1:3	1.5	2.30%
CF-5-NSP	3D nanostructured	1:5	1.2	1.91%

CF-1-NSP was found to be 2.8% which is the highest value among all 3D nanostructured devices as well as planar devices. The photoconversion efficiency (η_c) of CF-1-NSP is 2.25 times higher than CF-1-P and 4.17 times higher than pure hematite. The detailed values of photocurrent density and photoconversion efficiencies are given in Table 2.

CONCLUSIONS

In summary, $CuFe_2O_4/Fe_2O_3$ composite thin films were successfully deposited on plane FTO coated glass and 3D array of nanospikes. These thin films were then tested as anode material for light assisted electrolysis of water. Highest activity of water oxidation is achieved by composite CF-1 having 1:1 ratio of $CuFe_2O_4$ and Fe_2O_3. The photogenerated electrons in Fe_2O_3 travel to the outer circuit via valence and conduction band of $CuFe_2O_4$ in Z-scheme manner leading to the better separation of photogenerated electrons and holes which result superior photoelectrochemical properties of $CuFe_2O_4/Fe_2O_3$ composite. The photocurrent density has been further enhanced by increased surface area and better absorption of simulated sunlight upon depositing $CuFe_2O_4/Fe_2O_3$ composite thin film on 3D nanospikes. The current work is a step ahead in improving the efficiency of hematite thin film toward achieving the desired level in order to make it practically applicable.

ASSOCIATED CONTENT

Supporting Information

The Supporting Information is available free of charge on the ACS Publications website at DOI: 10.1021/acsami.6b12460.

> XRF results, optical images of prepared electrodes, EDS analysis, UV−vis absorption spectra of composite films, and HRTEM image of $CuFe_2O_4/\alpha\text{-}Fe_2O_3$ nanosheets (PDF)

AUTHOR INFORMATION

Corresponding Authors

*E-mail: eezfan@ust.hk.

*E-mail: manadeem@qau.edu.pk; Telephone: +92-51-9064-2062.

ORCID

Aashir Waleed: 0000-0002-6929-8373

Muhammad Arif Nadeem: 0000-0003-0738-9349

Notes

The authors declare no competing financial interest.

ACKNOWLEDGMENTS

This work is supported by Higher Education Commission (HEC) of Pakistan (No. 20-2704/NRPU/R&D/HEC/12). S.H. acknowledges the IRSIP scholarship of Higher Education Commission (HEC) of Pakistan for financial support while carrying out the research work in the Hong Kong University of Science and Technology.

REFERENCES

(1) Wang, G.; Ling, Y.; Wheeler, D. A.; George, K. E. N.; Horsley, K.; Heske, C.; Zhang, J. Z.; Li, Y. Facile Synthesis of Highly Photoactive α-Fe_2O_3-Based Films for Water Oxidation. *Nano Lett.* **2011**, *11*, 3503−3509.

(2) Kumar, P.; Sharma, P.; Shrivastav, R.; Dass, S.; Satsangi, V. R. Electrodeposited Zirconium-Doped α-Fe_2O_3 Thin Film for Photoelectrochemical Water Splitting. *Int. J. Hydrogen Energy* **2011**, *36*, 2777−2784.

(3) Murphy, A. B.; Barnes, P. R. F.; Randeniya, L. K.; Plumb, I. C.; Grey, I. E.; Horne, M. D.; Glasscock, J. A. Efficiency of Solar Water Splitting Using Semiconductor Electrodes. *Int. J. Hydrogen Energy* **2006**, *31*, 1999−2017.

(4) Joly, A. G.; Williams, J. R.; Chambers, S. A.; Xiong, G.; Hess, W. P.; Laman, D. M. Carrier Dynamics in α-Fe_2O_3 (0001) Thin Films and Single Crystals Probed by Femtosecond Transient Absorption and Reflectivity. *J. Appl. Phys.* **2006**, *99*, 053521−053526.

(5) Cherepy, N. J.; Liston, D. B.; Lovejoy, J. A.; Deng, H. M.; Zhang, J. Z. J. Ultrafast Studies of Photoexcited Electron Dynamics in γ- and α-Fe_2O_3 Semiconductor Nanoparticles. *J. Phys. Chem. B* **1998**, *102*, 770−776.

(6) Khaselev, O.; Turner, A. Monolithic Photovoltaic-Photoelectrochemical Device for Hydrogen Production via Water Splitting. *Science* **1998**, *280*, 425−427.

(7) McDonald, K. J.; Choi, K.-S. Synthesis and Photoelectrochemical Properties of $Fe_2O_3/ZnFe_2O_4$ Composite Photoanodes for Use in Solar Water Oxidation. *Chem. Mater.* **2011**, *23*, 4863−4869.

(8) Yin, J.; Bie, L. J.; Yuan, Z. H. Photoelectrochemical Property of $ZnFe_2O_4/TiO_2$ Double- Layered Films. *Mater. Res. Bull.* **2007**, *42*, 1402−1406.

(9) Hou, Y.; Li, X. Y.; Zhao, Q. D.; Quan, X.; Chen, G. H. Electrochemical Method for Synthesis of a $ZnFe_2O_4/TiO_2$ Composite Nanotube Array Modified Electrode with Enhanced Photoelectrochemical Activity. *Adv. Funct. Mater.* **2010**, *20*, 2165−2174.

(10) Tahir, A. A.; Wijayantha, K. G. U. Photoelectrochemical Water Splitting at Nanostructured $ZnFe_2O_4$ Electrodes. *J. Photochem. Photobiol., A* **2010**, *216*, 119−125.

(11) Sartale, S. D.; Lokhande, C. D.; Muller, M. Photoelectrochemical Water Splitting at Nanostructured $ZnFe_2O_4$ Electrodes. *Mater. Chem. Phys.* **2003**, *80*, 120−128.

(12) Sun, Z.; Liu, L.; Jia, D.Z.; Pan, W. P. Simple Synthesis of $CuFe_2O_4$ Nanoparticles as Gas-Sensing Materials. *Sens. Actuators, B* **2007**, *125*, 144−148.

(13) Kang, K. S.; Kim, C. H.; Cho, W. C.; Bae, K. K.; Woo, S. W.; Park, C. S. Reduction Characteristics of $CuFe_2O_4$ and Fe_3O_4 by Methane; $CuFe_2O_4$ as an Oxidant for Two-step Thermochemical Methane Reforming. *Int. J. Hydrogen Energy* **2008**, *33*, 4560−4568.

(14) Kameoka, S.; Tanabe, T.; Tsai, A. P. Self-assembled Porous Nano-composite with High Catalytic Performance by Reduction of Tetragonal Spinel $CuFe_2O_4$. *Appl. Catal., A* **2010**, *375*, 163−171.

(15) Nasrallah, N.; Kebir, M.; Koudri, Z.; Trari, M. Photocatalytic Reduction of Cr(VI) on Thenovel Hetero-system $CuFe_2O_4$/CdS. *J. Hazard. Mater.* **2011**, *185*, 1398−1404.

(16) Selvan, R. K.; Kalaiselvi, N.; Augustin, C. O.; Doh, C. H.; Sanjeeviraja, C. $CuFe_2O_4/SnO_2$ Nanocomposites as Anodes for Li-ion Batteries. *J. Power Sources* **2006**, *157*, 522−527.

(17) Fedailaine, M.; Bellal, B.; Berkani, S.; Trari, M.; Abdi, A. Photoelectrochemical Characterization of the Spinel $CuFe_2O_4$. Application to Ni^{2+} Removal under Solar Light. *Environ. Processes.* **2016**, *3*, 387−396.

(18) Tamaura, Y.; Kojima, M.; Sano, T.; Hasegawa, N.; Tsuji, M.; Ueda, Y. Thermodynamic Evaluation of Water Splitting by a Cation-excessive (Ni, Mn) Ferrite. *Int. J. Hydrogen Energy* **1998**, *23*, 1185−1191.

(19) Tamaura, Y.; Steinfeld, A.; Kuhn, P.; Ehrensberger, K. Production of Solar Hydrogen by a Novel, 2-step, Water-splitting Thermochemical Cycle. *Energy* **1995**, *20*, 325−330.

(20) Kojima, M.; Sano, T.; Wada, Y.; Yamamoto, T.; Tsuji, M.; Tamaura, Y. Thermochemical Decomposition of H_2O to H_2 on Cation-excess Ferrite. *J. Phys. Chem. Solids* **1996**, *57*, 1757−1763.

(21) Zhang, P.; Yu, B.; Zhang, L. Mechanism of Oxygen Releasing of Copper Ferrite in the Formation of the Corresponding Oxygen-deficient Compound. *Sci. China, Ser. B: Chem.* **2009**, *52*, 101−108.

(22) Qiu, Y.; Leung, S.F.; Zhang, Q.; Hua, B.; Lin, Q.; Wei, Z.; Tsui, K. H.; Zhang, Y.; Yang, S.; Fan, Z. Efficient Photoelectrochemical Water Splitting with Ultrathin films of Hematite on Three Dimensional Nanophotonic Structures. *Nano Lett.* **2014**, *14*, 2123−2129.

(23) Zhu, M.; Meng, D.; Wang, C.; Diao, G. Facile Fabrication of Hierarchically Porous $CuFe_2O_4$ Nanospheres with Enhanced Capacitance Property. *ACS Appl. Mater. Interfaces* **2013**, *5*, 6030−6037.

(24) Bak, A.; Choi, W.; Park, H. Enhancing the Photoelectrochemical Performance of Hematite (α-Fe_2O_3) Electrodes by Cadmium Incorporation. *Appl. Catal., B* **2011**, *110*, 207−215.

(25) Tahir, D.; Tougaard, S. Electronic and Optical Properties of Cu, CuO and Cu_2O Studied by Electron Spectroscopy. *J. Phys.: Condens. Matter* **2012**, *24*, 175002.

(26) Ding, J.; Zhong, Q.; Zhang, S. Simultaneous Removal of NO_X and SO_2 with H_2O_2 over Fe Based Catalysts at Low Temperature. *RSC Adv.* **2014**, *4*, 5394−5398.

(27) Yang, J.; Bao, C.; Yu, T.; Hu, Y.; Luo, W.; Zhu, W.; Fu, G.; Li, Z.; Gao, H.; Li, F.; Zou, Z. Enhanced Performance of Photoelectrochemical Water Splitting with ITO@α-Fe_2O_3 Core−Shell Nanowire Array as Photoanod ACS. *ACS Appl. Mater. Interfaces* **2015**, *7*, 26482−26490.

(28) Hu, J.; Jiang, L.; Zhang, C.; Zhang, X.; Meng, Y.; Wang, X. *Appl. Phys. Lett.* **2014**, *104*, 151602.

(29) Li, J.; Qiu, Y.; Wei, Z.; Lin, Q.; Zhang, Q.; Yan, K.; Chen, H.; Xiao, S.; Fan, Z.; Yang, S. Three-dimensional Hexagonal Fluorine-doped Tin Oxide Nanocone Array: A Superior Light Harvesting Electrode for High Performance Photoelectrochemical Water Splitting. *Energy Environ. Sci.* **2014**, *7*, 3651−3658.

DOI: 10.1021/acsami.6b12460
ACS Appl. Mater. Interfaces 2016, 8, 35315−35322